Microstructure evolution during Directed-Energy deposition of X40CrMoV5-1 analysed by in situ Synchrotron X-ray Diffraction and Atom Probe Tomography

Antonio Carlos de Figueiredo Silveira[1], Lisa T. Belkacemi[1,2], Pedro José de Castro[1], Jérémy Epp[1,2], Rainer Fechte-Heinen[1,2]

[1]*Leibniz-Institut für Werkstofforientierte Technologien-IWT, Badgasteiner Street 3, 28359 Bremen, Germany.*
[2]*MAPEX Center for Materials and Processes, Universität Bremen, Bibliothekstr. 1, 28359, Bremen, Germany.*

The Intrinsic Heat Treatment (IHT) generated during Additive Manufacturing (AM) processes such as Laser-directed energy deposition (L-DED) creates a complex thermal history in metallic components. This is mainly caused by the heating and cooling cycles the microstructure is subjected to during the process, which significantly vary over the built direction. This leads to heterogeneous mechanical properties in the manufactured component. This work investigates the microstructure evolution during IHT, with a particular focus on the subsequent carbide formation. To achieve this, in situ High Energy X-Ray Diffraction (HEXRD) experiments were performed at the Beamline P07 of Petra III Synchrotron at DESY, Hamburg, during the L-DED process of X40CrMoV5-1 steel. Besides the AM-typical repetitive phase transition, consisting into a combination of melting, solidification and martensitic transformation, the precipitation sequence was investigated. Making use of the high energy and brillance of the synchrotron beam, a high peak/background intensity ratio was obtained, enabling the identification of precipitates during the deposition. Additionally, atom probe tomography (APT) analyses and thermodynamic simulations were also performed to characterize the nature of the precipitates at different regions of the manufactured samples. The main findings show that different carbides are preferably formed depending on the heating and cooling cycles the microstructure is subjected to. At early stages,when the deposited layer is close to the regions of interest, vanadium carbides are briefly observed during solidification. Further on, when the depositions are sufficiently far to cause repeated reaustenitization cycles, the formation of mainly Chromium carbides is favored. During tempering cycles, a clear increase in the carbide fraction is seen in combination with the decomposition of the retained austenite. By combining both synchrotron and APT results with thermodynamic simulations, the precipitation kinetics and sequence could be analyzed in detail, revealing the underlying mechanisms and chemical interactions which led to the observed carbide distribution, in terms of size and chemical composition.

Keywords: *Additive manufacturing, Synchrotron X-ray diffraction, Atom probe tomography, Tool Steel*

1. Introduction

Laser-Directed Energy Deposition (L-DED) is an additive manufacturing process where the metallic powder is carried through nozzles by a pressurized gas (usually argon) to a focal point where a high-intensity laser melts the material, generating a deposition layer. The layer-by-layer manufacturing process results in multiple heating and cooling cycles, known as Intrinsic Heat Treatment (IHT) or in situ heat treatment, which modifies the previously deposited material[(1,2)]. Due to the progressively upward movement of the deposition zone, these thermal cycles are not uniform over the component and might induce different microstructures over the height. Depending on how prone the alloy is to tempering and secondary hardening, the final part might obtain very heterogeneous mechanical properties [(3)]. For this reason, AM parts are usually post-heat treated, increasing the cost of a part.

One possible alternative is taking advantage of the IHT to favor precipitates in the microstructure, improving the mechanical properties and possibly avoiding the need for additional post-heat treatments. This approach has been recently explored in maraging[(4,5)] and precipitation hardening[(6)] steels. The main conclusion of these studies is that the IHT, printing parameters, and alloy modification can be used to improve and control the precipitation formation of NiAl and Cu nano precipitates.

Tool steels are another class of alloys that can benefit from this approach, given the well-known secondary hardening caused by the formation of Cr and V precipitates. However, the state of the art is primarily limited to post-mortem investigations or tracking the precipitate evolution during isothermal experiments.

This work aims to investigate the evolution of the precipitates during L-DED manufacturing of X40CrMoV5-1 steel samples through HEXRD and APT to characterize the chemical concentration and nature of the precipitates formed by the IHT.

2. Materials and methods

The in-situ L-DED experiments were performed at the Deutsches Elektronen- Synchrotron (DESY) on Beamline P07-EH3 of the PETRA III with a 97.6 KeV monochromatic X-ray beam. During the experiments, the diffraction patterns were recorded at different sample positions with time resolution of 10Hz. A detailed overview of the experimental setup and of the results can be found in[(1)]. After the experiments, selected samples were investigated by Electron microprobe Analysis (EMPA), Scanning electron microscopy (SEM), and Atom Probe Tomography (APT).

For the synchrotron data analysis, the diffracted patterns were integrated with the software PyFai, and the phases were quantified with the convoluted-based Rietveld refinement software Topas Academic 6. To account for the detector aberrations and instrumental contributions, a NIST standard LaB6 powder was also measured and accounted for in the data integration and refinement. In addition to the main phases, the following crystal structure phases were

also considered: M_3C, M_7C_3, $M_{23}C_6$, MC, M_8C_7, Fe_3O_4, and Fe_2O_3.

For the APT analysis, LEAP 5000 XR from Cameca was used in Laser mode and the data were analyzed with the software APSuite 6.1.

3. Results

3.1 Temperature and carbide evolution during L-DED

Based on the lattice parameter of austenite, an estimated temperature can be calculated based on the work of Onink[8] which is shown in our previous work[1]. Figure 1 shows the temperature history at the bottom of the wall (position 0%) overlaid with the phase fraction of the most significant carbide phase structures.

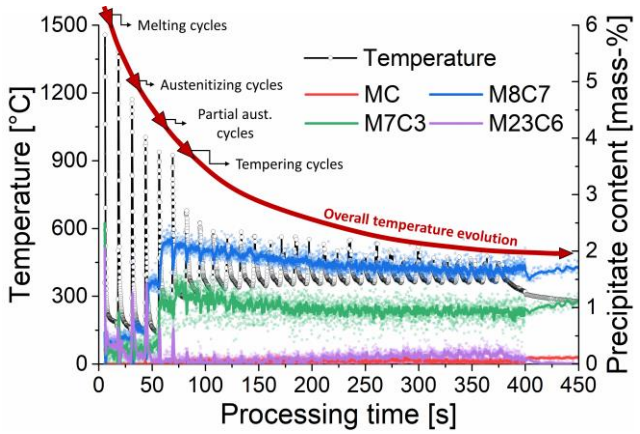

Figure 1. Temperature (black) and carbide fraction (red, blue, green, and purple) evolution during L-DED in situ experiments at position 0% of the wall.

During the deposition, the melting liquid solidifies primarily into austenite and afterwards transforms into martensite while some austenite is retained. During the next depositions, the microstructure is either remelted, reaustenitized, or tempered. The type of phase transformations is related to the distance of the deposition region from the investigated zone, which determines the heat input. Based on the temperature evolution in Figure 1, it can be seen that at the two initial thermal cycles, the temperature exceeds 1400°C, indicating that the deposed material was remelted after the initial deposition. During this period, the Rietveld refinement could not detect significant carbide phases. The same trend is observed during the austenitizing cycles. However, a sharp increase between 1% to 2% of M_7C_3 and V_8C_7 is seen when partial austenitizing cycles start to take place. During these cycles, the peak temperatures are between 860 and 960 °C, corresponding to the Ac_{1b} and Ac_{1e} for this steel, respectively. As the tempering cycles occur, the temperatures remain between 600 to 300°C, and the fraction of these two carbides decrease slightly, while a small increase in $M_{23}C_6$ can be observed.

3.2 Carbides quantifications by APT

After the in situ experiments, APT tips from the exact position of the experiment were extracted from the sample by targeted FIB-preparation. Figure 2 shows a reconstructed tip from position 0%.

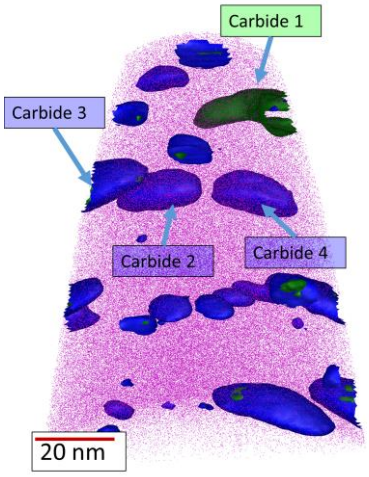

Figure 2. Reconstructed tip from the bottom of the wall (position 0%). A V (blue) and a Cr (green) iso-surfaces are overlayed with the Fe ions (purple dots).

Several carbides are mainly associated with either V but also one associated with Cr. The V carbides have an ellipsoid/disc shape with an average diameter of 6.7 ± 0.5 nm, while the Cr ones have a more elongated shape. Additionally, the C distribution seems to be majorly accumulated into these precipitates, and no other features are observed. The chemical composition of the highlighted carbides is shown in Table 1. With the presence of carbides, the C quantification is usually underestimated due to occurance of multiple events and C molecules[9]. To compensate for this deficiency, the carbon content can be corrected based on the natural abundance, as proposed by Thuvander et al.[7]. Carbide 1 is mainly associated with Cr and Fe and has a stoichiometry M:C close to $M_{23}C_6$. The other carbides, primarily associated with V, have a significant fraction of N and a stoichiometry closer lower than the stoichiometry usually found in VC or V_8C_7 carbides.

Table 1. Carbide chemical composition.

Carbide	V	Cr	Mo	Fe	C	N	M:C
1	2.3	16.7	1.0	58.2	21	-	0.27
2	42.4	8.1	9.0	-	34.8	4.5	0.65
3	42.0	7.2	9.0	-	36.2	4.5	0.69
4	43.8	9.1	8.1	-	33.9	3.7	0.60

4. Discussion

Despite the corrections applied to the APT findings, the stoichiometry do not fully match the identified phases in the HEXRD in situ experiments, particularly for the V-carbides. The main reason for this is the presence of vacancies in these carbides, which are not considered in the APT and directly reduce the chemical stoichiometry of the phases[10]. Regarding the Cr carbides, the highlighted carbide matches one of the $M_{23}C_6$ which is also found in the HEXRD, however, the main observed Cr carbides (M_7C_3) was not found in APT.

Based on the in situ experiments, the V carbides are mainly formed during the partial austenitizing cycles. These have a higher temperature stability and are less prone

to coalesce and grow. Therefore, these thermal cycles can be advantageous in promoting the formation of these carbides, which are further on do not coarsen, creating a positive impact on the mechanical properties of the microstructure.

4. Conclusions

1. The in situ experiments showed an increase in V and Cr carbides during partial austenitizing.
2. The APT analysis showed a high density of V carbides with a range of 6 nm size but also the presence of elongated Cr carbides.
3. The correction of the C content in the carbides resulted in a stoichiometry of the Cr carbide close to the expected M23C6, however the stoichiometry of the V carbides is lower than the usually observed VC and V8C7, which is associated with the presence of vacancies in these phases

(1) A.C. de F. Silveira, R. Fechte-Heinen, J. Epp, Microstructure evolution during laser-directed energy deposition of tool steel by in situ synchrotron X-ray diffraction, Addit. Manuf. 63 (2023) 103408. https://doi.org/10.1016/j.addma.2023.103408.

(2) J. Epp, J. Dong, H. Meyer, A. Bohlen, Analysis of cyclic phase transformations during additive manufacturing of hardenable tool steel by in-situ X-ray diffraction experiments, Scr. Mater. 177 (2020) 27–31. https://doi.org/10.1016/j.scriptamat.2019.09.021.

(3) S. Amirabdollahian, F. Deirmina, M. Pellizzari, P. Bosetti, A. Molinari, Tempering behavior of a direct laser deposited hot work tool steel: Influence of quenching on secondary hardening and microstructure, Mater. Sci. Eng. A. 814 (2021) 141126. https://doi.org/10.1016/j.msea.2021.141126.

(4) P. Kürnsteiner, M.B. Wilms, A. Weisheit, P. Barriobero-Vila, E.A. Jägle, D. Raabe, Massive nanoprecipitation in an Fe-19Ni-xAl maraging steel triggered by the intrinsic heat treatment during laser metal deposition, Acta Mater. 129 (2017) 52–60. https://doi.org/10.1016/j.actamat.2017.02.069.

(5) S. Amirabdollahian, F. Deirmina, L. Harris, R. Siriki, M. Pellizzari, P. Bosetti, A. Molinari, Towards controlling intrinsic heat treatment of maraging steel during laser directed energy deposition, Scr. Mater. 201 (2021) 113973. https://doi.org/10.1016/j.scriptamat.2021.113973.

(6) Q. Guo, M. Qu, C.A. Chuang, L. Xiong, A. Nabaa, Z.A. Young, Y. Ren, P. Kenesei, F. Zhang, L. Chen, Phase transformation dynamics guided alloy development for additive manufacturing, Addit. Manuf. 59 (2022) 103068. https://doi.org/10.1016/j.addma.2022.103068.

(7) M. Thuvander, J. Weidow, J. Angseryd, L.K.L. Falk, F. Liu, M. Sonestedt, K. Stiller, H.-O. Andrén, Quantitative atom probe analysis of carbides, Ultramicroscopy. 111 (2011) 604–608. https://doi.org/10.1016/j.ultramic.2010.12.024.

(8) M. Onink, C.M. Brakman, F.D. Tichelaar, E.J. Mittemeijer, S. van der Zwaag, J.H. Root, N.B. Konyer, The lattice parameters of austenite and ferrite in Fe-C alloys as functions of carbon concentration and temperature, Scr. Metall. Mater. 29 (1993) 1011–1016. https://doi.org/10.1016/0956-716X(93)90169-S.

(9) L. Yao, B. Gault, J.M. Cairney, S.P. Ringer, On the multiplicity of field evaporation events in atom probe: A new dimension to the analysis of mass spectra, Philos. Mag. Lett. 90 (2010) 121–129. https://doi.org/10.1080/09500830903472997.

(10) C. Ioannidou, A. Navarro-López, A. Rijkenberg, R.M. Dalgliesh, S. Koelling, C. Pappas, J. Sietsma, A.A. van Well, S. Erik Offerman, Evolution of the precipitate composition during annealing of vanadium micro-alloyed steels by in-situ SANS, Acta Mater. 201 (2020) 217–230. https://doi.org/10.1016/j.actamat.2020.09.083.